

Local and global measurements in trickle bed reactor, Part 1: Pressure drop and flow regime map

Shripad T.Revankar^{1,2*}, Xiangcheng Kong¹

¹School of Nuclear Engineering, Purdue University, West Lafayette, IN 47907, (USA)

²Division of Advanced Nuclear Engineering, POSTECH, Pohang, Gyeongbuk 790-784, Republic of Korea, (KOREA)

E-mail : shripad@purdue.edu; shripad@postech.ac.kr

ABSTRACT

A trickle bed test facility was designed and constructed with impedance based global bed void and liquid hold up measurement. Single phase flow and two phase flow characterization of the test loop was performed by air and water concurrent down flow in the bed. The flow regime in the bed was observed and recorded with high speed video camera. Flow regime map was developed. Five flow regimes were identified, trickling, wavy, transitional, pulsing and bubble flow. Pressure drop measurements in the bed were also obtained for various flow regimes in the bed. The data of the pressure drop and flow regime maps were compared with previous works and a good agreement was found between and present and previous works.

© 2015 Trade Science Inc. - INDIA

KEYWORDS

Trickle bed reactor;
Packed bed air-water flow;
Impedance probe;
Flow regime map;
Pressure drop.

INTRODUCTION

Trickle-bed reactors, in which a gas and a liquid flow concurrently downward over a randomly packed stationary bed, are widely used in variety of gas-liquid-solid catalytic reactions including petroleum and petrochemical industries. Its application mainly concerns the processing with hydrogen of various petroleum fractions, in particular the hydrodesulphurization or hydrocracking of lubricating oils^[1]. A number of industrial reactors have operated near the trickling-to-pulsing transitions. An understanding of the conditions at which transition from one regime to another occurs, as well as the two-phase flow parameters in each of these regimes, is of fundamental importance in the design and scale-up of these reactors. In general, gravitational, capillary, and viscous forces drive flow in porous media. Though recently various studies have been conducted for two-

phase flow through packed bed to understand the mechanisms governing the flow regime transition, pressure drop, void and interfacial area distribution, there are few published works available on this topic with detailed local measurements. The bed characterization is generally done through macro scale parameters such as total bed pressure drop, liquid hold up and total void. It should be noted that the macro scale parameters are rooted in the micro scale, where two-phases compete for the void space.

In view of this, an experimental study is performed where systematic experiments are conducted for the gas-liquid two-phase flow in a packed bed with local as well as global instrumentation to characterize the flow. This paper is first part of two parts series and presents experimental results on pressure drop and flow regime map. Part two paper present further results on local measurement on void fraction, film thickness on the

packing and characteristics of pulses.

FLOW REGIME AND FLOW MAPS

The most common method for detecting flow regime transition involves the observation of the flow pattern through transparent column walls. The subjective nature of the qualitative method has resulted in the variety of names reported for the different flow regimes and the uncertainty in flow regime boundaries.

There are many different flow regime definitions in literature. These flow regimes can be divided into two basic categories: low interaction regime and high interaction regime. The low interaction regime is also called trickling flow regime, in which both liquid and gas flow continuously. High interaction simply means liquid and gas interact each other at a higher level. Further classifications can be made within high interaction regime which is different for foaming or nonfoaming liquid. In this project, only nonfoaming liquid is concerned.

Four flow regimes are fundamentally defined by the criteria of continuity of gas and liquid. Trickling, both gas and liquid are continuous; Spray, only gas is continuous; Pulsing, both are not continuous; Bubble, only liquid is continuous. Figure 1 shows four basic flow patterns. Based on these four flow regime definitions, additional flow regime classifications can be made. Houlob^[2] separated wavy flow regime from trickling flow regime. In wavy flow, the liquid is flowing as a film or rivulet but is not steady, a wave of the film can be observed. Weekman et al.^[3] defined a transition or ripple flow regime between the trickling and pulsing flow regimes. He defined it as the liquid appearing to be in turbulent flow and giving the visual impression of many small ripples. Occasional pulses may be observed near the bottom of the column.

Similarly, Sato and Hirose^[4] also defined a transitional flow regime in which pulse happened partly in the lower portion of the column. Talmor^[5] separated pulsing regime into a pulsing regime and a bubbling/pulsing regime. In the bubbling/pulsing regime, both bubbling in the water slug and pulsing can be observed. Ng^[6] added a dispersed bubble flow regime in which bubbles become highly irregular in shape while in the bubble flow regime bubbles are only slightly elongated.

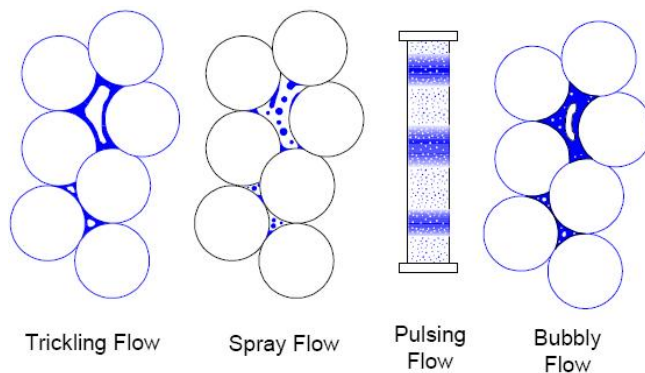


Figure 1 : Schematic of different flow regimes

Above all, no good quantitative profile for flow regime transitions can be drawn when there are only qualitative definitions for transitions. So there are two solutions to this contradiction. First, give quantitative definitions to flow regime transitions. Chou et al.^[7] use this approach. In his article, the flow regime transition was defined as the condition at which a slight increase in gas or liquid flow rate caused a sharp increase in the wall pressure fluctuation. Second, use the neural network and fuzzy logic method of Artificial Intelligence Technology. Now Artificial Intelligence Technology is being developed extensively and the use of neural network in identifying flow regimes has been studied and applied in the nuclear engineering field.

The effect of the distribution head should be considered when the flow regime map is produced from experiments. The distribution head is installed at upstream of the test section to provide uniform liquid and/or gas flow. Some researchers like Sato and Hirose^[8] provided a detailed description of this component since they realized it can exert a large influence on initial conditions of the test section. Flow regime transition is a kind of instability, so initial conditions are very important for the later development. Some researchers added a separated mixing section between the distribution head and the test section. Such a component can greatly reduce the end effect at the inlet of the test section.

With all of the above considerations, it seems to not be very meaningful to compare various flow maps from different researchers. Accurate analyses and direct conclusions from comparison of different researchers' work are not reasonable. However, this thesis shows the comparison between present and previous data to provide readers with a rough impression. The general

Full Paper

information of experimental flow maps by previous researchers is listed in TABLE 1 (4,5,7-13).

In TABLE 1, U is superficial velocity, G and L are gas and liquid mass fluxes, Re is the Reynold numbers, and subscripts g and l are for gas and liquid respectively. The apremetera λ and Ψ are known as Baker coordinates and are given as, $\lambda = (\rho_g/\rho_a)^{0.5}(\rho_l/\rho_w)^{0.5}$ and $\Psi = (\sigma_w/\sigma_l)(\rho_w/\rho_l)^{0.66}(\mu_w/\mu_l)^{0.33}$, μ is viscosity and subscripts a and w correspond to air and water respectively. Sato and Hirose^[4] introduced the transitional flow regime between pulsing and gas continuous flow regimes. When pulsing is generated partly in the lower portion of the test section, they called it as the transitional flow regime. If the pulse spreads over the whole test section, it is the pulsing flow regime. In 1977, Talmor^[5] presented a flow map in which he used superficial volumetric gas-to-liquid ratio vs. the ratio of driving force to resistance force. Volumetric gas-to-liquid ratio is the same as superficial velocity ratio.

In the two-phase flow field, superficial velocity is same as the term of volumetric flux. The ratio of driving force to resistance force can be expressed as follows;

$$\frac{\text{Driving Force}}{\text{Resistance Force}} = \frac{\text{Inertia}(I)+\text{Gravity}(G)}{\text{Interface}(S)+\text{Viscous}(V)} = \frac{1+G/I}{S/I+V/I} = \frac{1+1/Fr}{1/We+1/Re} \quad (1)$$

Here Fr is Froud number and Re is Reynold number. However, he used Weber number (We) instead of

the inverse of Weber number in the denominator of above equation. This means he considered the interfacial resistance as the square of inertia divided by surface tension as shown below.

$$\frac{\text{Driving Force}}{\text{Resistance Force}} = \frac{\text{Inertia}(I)+\text{Gravity}(G)}{\text{Interface}(I^2/S)+\text{Viscous}(V)} = \frac{1+1/Fr}{We+1/Re} \quad (2)$$

In his article, he explained that for successful flow mapping, surface tension and viscosity have opposite effects on the force ratio. Although the physical meaning of each of the dimensionless number coordinate is clear, the physical correlation between the ratio and the regime transition is implicit. Various forces perform different roles in the instability. So the idea presented by Talmor^[5] to use a dimensionless number from various forces to show flow maps more clearly is good. But those forces should be analyzed more carefully. Talmor^[5] himself pointed out that the mechanism of transition between each flow regime is expected to be different and no single choice of general flow map coordinates will collapse all transition zones into sharp boundaries. In the field of the research for two-phase flow regime in tube, a similar opinion was held by Al-Sheikh et al.^[4]; no two dimensionless groups characterized all of the transitions and all of the data.

Many parameters have significant effect on the transition from trickling to pulsing flow. Gianetto^[15] and

TABLE 1 : Experimental stuides in trickle bed reactor flow regimes

| Researcher | Packing Shape | Packing size (mm) | Column ID (cm) | Porosity | Map Coordinate | Units | Regime Classification | Transition Criteria or other comments about flow regime |
|--------------------|---------------------------------|--------------------------------|--------------------|---------------------------|-----------------------------------|--------------------------------------|--|--|
| Chou (1977) | Sphere | 2.9 | 6.35 | 0.39 | U_g-U_l | cm/s | Gas continuous - Pulsing | A slight flow rate increase caused a sharp increase in the pressure fluctuation |
| Drinkenburg (1983) | Raschig Ring | 2.5x2.5 4x4 | 5, 10, 20 | 0.6 0.74 | U_g-U_l | m/s | Gas continuous - Pulsing | The first occurrence of pulses at the bottom of the column was taken as the transition point |
| Sato (1973) | Sphere | 8.01 | 12.2 | 0.382 | G-L | $\text{Kg/m}^2\text{s}$ | Gas continuous- Transitional-Pulse- Dispersed Bubble | Transitional flow: pulse is observed partly in the lower portion of the column. Pulse flow: pulse spreads over the whole column. |
| Charpentier (1975) | Sphere | 3 | 5 | 0.39 | $L\lambda\psi/G-G/\lambda$ | $1-\text{Kg/m}^2\text{hr}$ | Trickling - Pulsing | Transition line means transition regime. |
| Weekman (1964) | Sphere | 3.78, 4.75, 6.48 | 3 inch I.D pipe | 0.378, 0.390, 0.430 | G-L | $\text{LB}/(\text{HR})(\text{FT})^2$ | Trickling - Transition - Pulsing | Transition: liquid in turbulent flow and many small ripples observed. Occasional pulses occurred near the bottom of the column |
| Talmor (1977) | Cylinder | 3.5 | 29.2 | 0.366 | Driving force/ resistive force | 1 | Liquid continuous- Bubbling and pulsing- Pulsing-Gas continuous- | Bubbling and pulsing: Both bubbling and pulsing can be observed |
| Specchia (1977) | Sphere Cylinder Cylinder | 6 5.4x5.4 2.7x2.7 | 8 | 0.4, 0.37, 0.38 | $L\lambda\psi/G-G/\lambda$ | $1-\text{Kg/m}^2\text{hr}$ | Poor interaction - High interaction | Same as Charpentier |
| Fukushima (1978) | Rashig Ring Sphere Sphere | 3/8 inch 1/2 inch 1 inch | 11.4, 20 | 0.67, 0.37, 0.39 | Re_g-Re_l | 1 | Trickle-wavy-spray- pulse-dispersed bubble | Measure IAC from oxygen absorption into sodium sulfite solution with cobaltous chloride as a homogeneous catalyst |
| Turpin (1967) | Tabula alumina | 7.62, 8.23 | 2, 4, 6 inch | 0.4 | L/G-G | $\text{LB}/(\text{HR})(\text{FT})^2$ | Spray - Slug - Bubble | No abrupt change of pressure drop for any of the transitions from one flow type to another. |
| Present | Sphere | 6 | 6.92 | 0.37 | G-L | m/s | Tricking, wavy, transitional, pulse, bubbly | Transition criterion based local and global instrumentation on void fraction, film thickness |

Charpentier et al.^[10] incorporated the interfacial surface tension, the liquid viscosity, the densities of the gas and the liquid, and the packing porosity into flow maps empirically. These new parameters for flow map were originally proposed by Baker^[16] for two-phase flow in horizontal pipes. From Charpentier's^[10] experiment, the transition lines between trickling and pulsing flow regime for different working fluid are identical with new parameter.

EXPERIMENTS

The experimental program involved the design of the test section, instrument development, instrument calibration and testing, experiment procedure, and data processing. For the first phase of the project, an experiment loop was developed to study the downward concurrent two-phase flow in a packed bed.

Test loop

In Figure 2 the schematic of the test experimental loop is shown. The loop consists of the test section, water tank, water pump, air flow line and instrumentations.

A 1/2 hp centrifugal pump is used to pump water to the packed bed. The laboratory compressed air supply is used with copper piping.

The test section consists of the inlet distribution head where air and water are mixed and injected into the packed bed. The distribution head has 13 gas tubes that open at the top plenum where air is injected. The air tubes inject air stream directly to the inlet of the bed. The water is fed to the lower plenum with three inlet symmetrical located on the lower plenum. There are 24 tubes that take the water from the lower plenum and inject into the inlet of the bed where it mixes uniformly with the air stream.

The packed bed test section is made of the transparent acrylic tube. The ID of the tube is 69 mm with wall thickness of 3.3 mm. The length of the test section is 1.52 m.

Packing particles are 6mm spherical glass beads. The shape and size are typical for previous research works (see TABLE 1). In the present loop, no separated mixing section is used downstream of the distribution head. The length of the test section of the present

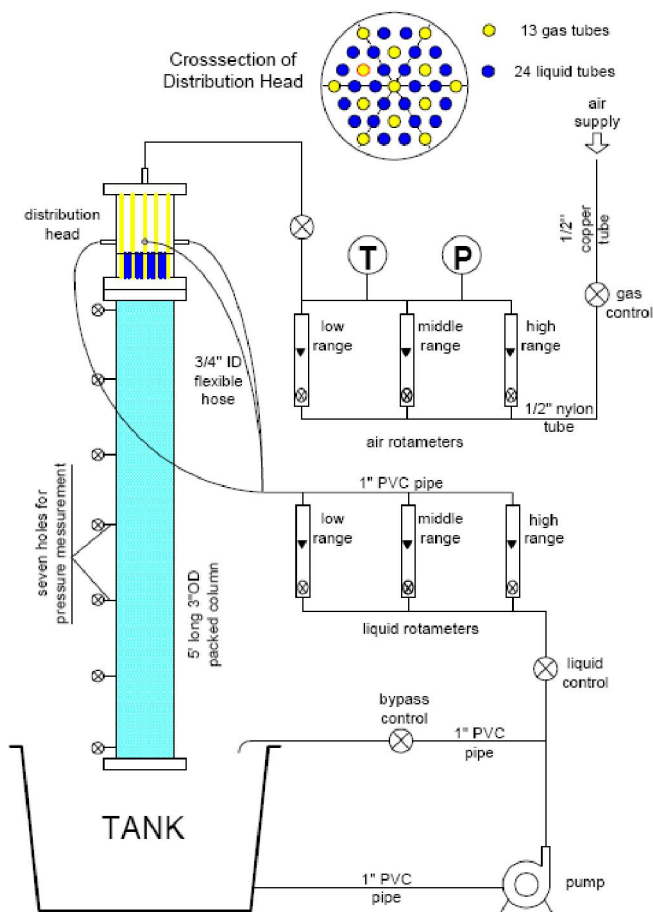


Figure 2 : Schematic of experimental loop

loop is longer than normal experimental packed bed and the upper region of the present test section is used as a mixing region. The bed porosity was obtained by counting a sample of beads and weighing. For 500 beads the weight was 142 grams with single bead weight of 0.284 grams. This measurement was repeated once. Using this method the total numbers of beads in the packed bed were obtained. In TABLE 2 the data of the bed porosity measurements is given.

The air flow rate and the water flow rates are measured each with a set of three rotameters connected in parallel. Each rotameter have a decade range so a three decade scale of flow range (low, middle and high) can be covered with these rotameters. The ranges of rotameters are:

- Gas low range: 0.4 – 5 LPM
- Liquid low range: 40 – 400 CCM
- Gas middle range: 4 – 50 LPM
- Liquid middle range: 0.1 – 1 GPM
- Gas high range: 2 – 20 SCFM
- Liquid high range: 1 – 10 GPM

TABLE 2 : Packed bed porosity

| The number of the beads | 31957 |
|---|------------|
| The length of test section corresponding the packing | 1.536 m |
| The length of test section pressure drop from the first inlet to atmosphere | 1.506 m |
| Volume of one bead | 0.11310 ml |
| Volume of all the beads | 3614.3 ml |
| Volume of test section holding beads | 5797.4 ml |
| Porosity | 0.377 |

Thermocouple and bourdon pressure gage are installed near the air rotameters. Data acquisition system includes the DAS-1801ST data acquisition board and STA-1800U screw terminal accessory board. A high speed video camera (10000 FPS) was used for flow regime visualization. Other instrument used included impedance meter to measure the bed cross section averaged void fraction the design of which is give in next section.

Impenace meter

The impedance meter is half circle plate type and was specially designed for the packed bed. The design is similar to the one used for pipe flow^[17]. Six signal processing circuits were built, similar to those described by Revankar et al.^[17]. The probe outputs were taken to the signal processing circuits, whose outputs could be either displayed on an oscilloscope or recorded using a high speed data logger. The voltage output of the probe-circuit combination was initially assumed to be linear with void fraction. Since resistance and capacitance are both functions of void distribution, the validity of this assumption was checked by calibration tests and computer modeling of the probe's response to various void distributions. The impedance varies depending on the void fraction in the two-phase air-water flow.

The design of impedance meter and a picture of installed meter is shown in Figure 3. Two pieces of aluminum foil are mounted by insulation tape on the surface of the test section. Vacuum grease was used to prevent air gap exist between the wall and the foil. To decide the height of the foil, experiments were conducted and result shows that the greater the height the more sensitive the meter. However, the volume averaged void fraction from impedance meter lost its accuracy for one certain position when the height of the foil is too large. Design is based on a compromise between

the accuracy and sensitivity and 8 cm were at last set for all impedance meters. Other researchers used shielding to remove influence from environment. For present experiment, shielding was tried and it was found that shielding also decreased the sensitivity since it provide one more capacitance link between the two electrodes

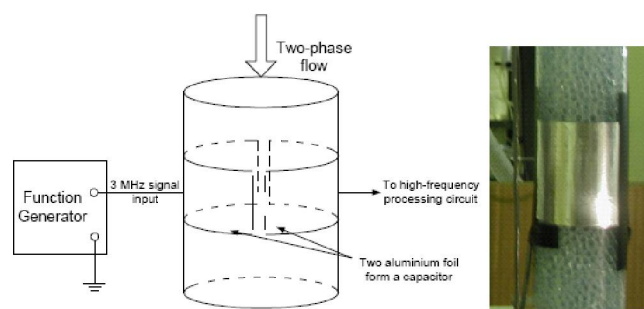


Figure 3 : Design of impedance meter and picture of install meter on packed bed

One of the advantages of impedance meter is its fast response. The meter was calibrated using known void fraction inserted in test section and a calibraton curve is shown in Figure 4.

There are mainly two sources of electrical noise except environment: the impedance meter circuit and the channel interference of the data acquisition system. Output from impedance meter circuit was supposed to be DC signal while input to the circuit is 3MHz high frequency signal. Small amplitude 3MHz noise still exists in the output. The DAS-1801ST board has sixteen channels. The noise level increased significantly when most of the channels working at the same time. To eliminate the noise of the signal from data acquisition system, a wavelet analysis method was applied. Five level decompositions are applied to the original signal. High frequency electric noises were extracted out by discrete wavelet transform^[18]. In Figure 4., S is the original voltage signal from impedance meter #4 in three seconds; a5 is the low frequency hydraulic content left,

others are different high frequency extractions. The flow condition is water superficial velocity $U_f=0.0067\text{m/s}$, air superficial velocity $U_g=1.125\text{m/s}$.

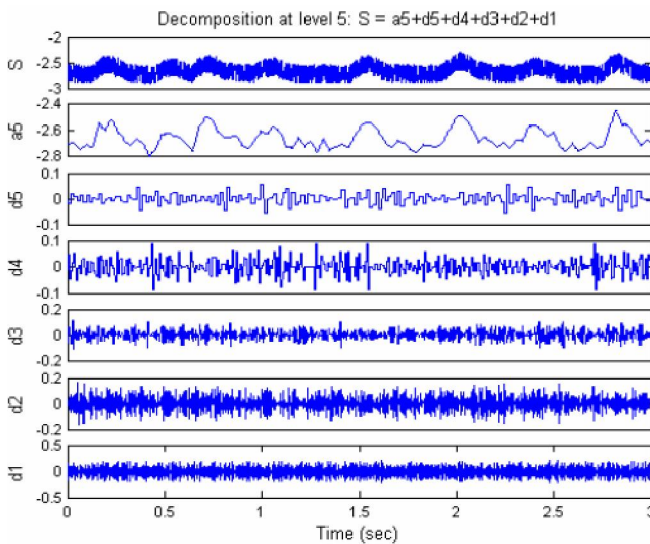


Figure 4 : Wavelet analysis of the impedance meter signal

Experimental procedure

Test preparation included adjusting the water conductivity to $200\mu\text{s/cm}$, purging the DP sensor lines, keeping the electronics powered, and the laboratory air compressor on. Single phase air flow and single phase water flow experiment were done for reference. Each of them was repeated three times for accuracy. For the tests first the water pump was started and the water flow rate was set by using the control valves on the water rotameters. Once the required water flow rate was established, the air flow was started and the flow rate is controlled with the rotameter control valves. After the two-phase flow became stable, signals from instruemn and from high speed camera were recorded. The sample frequency of the data acquisition system was set as one kilohertz. A one minute signal was recorded for each flow condition. The air flow rate was increased in sequence for a fixed water flow rate until the maximum air flow rate was reached. Then the data were taken in decreasing order of air flow rates. This was repeated for different water flow rate.

EXPERIMENTAL RESULTS

Single phase flow

In order to characterize the packed bed single phase

flow, pressure drop experiments were performed for single phase water and air respectively. In order to present the single phase data Ergun^[19] equation for the pressure drop is used. The Ergun equation is:

$$\frac{\Delta P}{L} = 150 \frac{(1-\varepsilon)^2}{\varepsilon^3} \frac{\mu U}{d_p^2} + 1.75 \frac{1-\varepsilon}{\varepsilon^3} \frac{\rho U^2}{d_p} \quad (3)$$

where, ΔP ; combined effect of static pressure and gravitational force,

$$\Delta P = \Delta p + \rho g h, \quad (4)$$

h is the distance vertically upward; U ; superficial velocity; d_p ; mean particle diameter, μ ; fluid viscosity, ρ ; fluid density, ε ; bedporosity and L ; bed height.

The two Ergun constants are: $k_1=150$, $k_2=1.75$. Usually k_1 is called the Kozeny-Carman constant, k_2 the Burke-Plummer constant. The physical meaning of the first term in the right side of the equation is pressure drop due to the viscous force at the laminar flow while the second term is the pressure drop due to the shear stress by the packing surface at the turbulent flow. Holub^[2] made a summary table of all the previous Ergun constants. The k_1 ranges from 100 to 850 while k_2 ranges from 0.8 to 2.4. Hasseni et al.^[20] studied single-phase flow with many kinds of gas and liquid. His studies show that Kozeny-Carman constant varies significantly between gas flow and liquid flow. For gas flow, the superficial velocity changes through the packed bed for the compressible fluid. In non-dimensional form the Ergun equation is given as^[21]:

$$\left(\frac{\Delta P \rho}{G^2} \right) \left(\frac{d_p}{L} \right) \left(\frac{\varepsilon^3}{1-\varepsilon} \right) = 150 \frac{1-\varepsilon}{d_p G / \mu} + 1.75 \quad (5)$$

where G is mass flux. For small ΔP , the data fits the Ergun equation when the mass flux is constant and gas density is calculated by the arithmetic average of inlet and outlet pressure. For large ΔP , local pressure gradient should be used considered and local density has to be used to determine Ergun constants. Hasseni et al^[20] experiment showed no influence of the gas density and the total pressure on the two constants. The term on left hand side $\left(\frac{\Delta P \rho}{G^2} \right) \left(\frac{d_p}{L} \right) \left(\frac{\varepsilon^3}{1-\varepsilon} \right)$ is called as the modified

friction factor f , and the term on right hand side $\frac{G d_p}{\mu(1-\varepsilon)}$ is called modified Reynolds number Re , for flow in packed bed. Experimentally the Ergun constants are

Full Paper

obtained by fitting experiment data in below equation:

$$f = k_1 / Re + k_2 \quad (6)$$

Current experimental results for water and air flow in the packed bed are shown in terms of f and Re in Figure 5. Since the lower water flow range was not possible the Kozeny-Carman constant cannot be obtained from this data. The Burke-Plummer constant from the Figures 5 is 1.3.

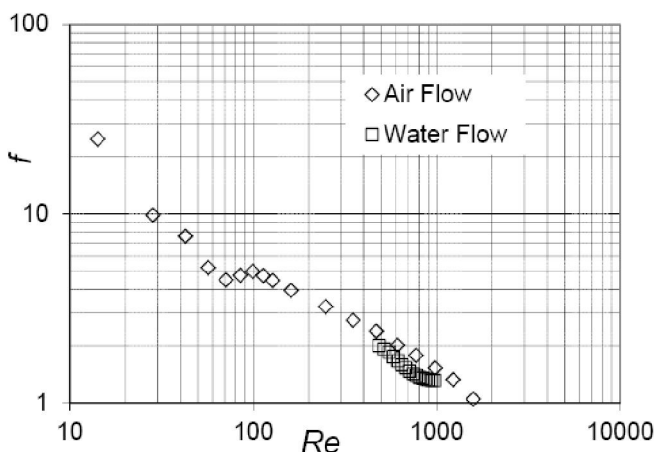


Figure 5 : Friction factor for single phase air and water flow in packed bed

For small pressure drop, error due to the compressibility of air is negligible. With the first 5 points, the linear fitting with least square method shows that the Blake-Kozeny constant is 309. The result show the Burke-Plummer constant for air flow is 1.26. This compares well with the result of water flow test where a value of 1.3 was obtained for Burke-Plummer constant. These two constants are typical in comparison with other researchers' value. For reference, good summary tables of packed bed parameters can be found in the paper of Holub^[2].

Two-phase flow

Two-phase concurrent down flow tests were carried out for various air-water flow combinations. With different combination of air-water flow the following flow regimes were obtained: trickling, wavy, pulsing, bubbly, and transitional flow. A high speed video camera was used to take images of the flow in the test section. Observation point is close to impedance meter #4. Three speeds were used: 500, 250, and 30 frames per second (fps) depending on the phenomena. For highly agitated flow 500 fps was used. It should be noted

that these images show flow between packing and wall, not inside packing. To get more accurate local pictures inside the packing, endoscope measurements are planned. For the present analysis, the flow near wall and flow inside packing are assumed to be similar.

When the flow rates are small, researchers have described the flow as film or rivulet and named the flow regime trickling, channeled or low interaction. In this flow some fraction of the packing surface remains unwetted. The video images showed that in the trickling flow regime, the flow on packing surface is more like rivulets than smooth films. This is key information which should be accounted in the modeling of the trickling flow regime. The film thickness probe measurement will provide further data to this observation. For pulsing flow, water pulses run down along test section. The pulse speed can be calculated by dividing the travel distance of pulse by the time interval between pictures. The impedance meter transient void measurement can be used to confirm these measurements. In bubbly flow, From images it was observed that bubbles were not spherical shape in general. The bubbles were often elongated. Bubbly flow regime subdivided into bubbly flow with slightly elongated bubbles and dispersed bubbly flow with highly irregular bubbles in shapes. This bubble deformation is very important since the interfacial area for the irregular shape and elongated bubbles is larger compared to spherical bubbles. Hence in the modeling of bubbly flow this should be accounted.

Two phase flow pressure drop

Pressure gradient as a function of water volumetric flux is shown for different gas flow rate in Figure 6. Data of Drinkenburg^[9] are also shown for comparison. The Drinkenburg data are obtained from Raschig ring packing with 4mmx4mm size and in cylindrical column of diameter 5 cm and porosity 0.6. The present data is close to data of Drinkenburg.

In Figure 7., the two-phase pressure gradient is shown as a function of air volumetric flux for different liquid flow rates.

Flow regime map

The flow regimes for various combinations of air-water flow in the packed bed were based on direct visual observations and the images from the high speed

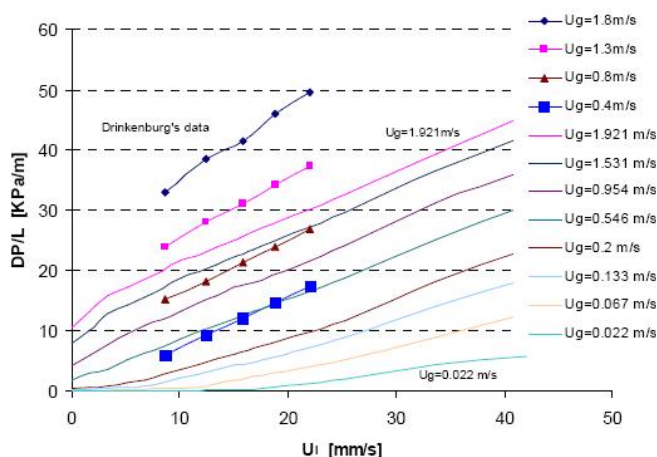


Figure 6 : Two-phase pressure gradient vs. water volumetric flux drinkenburg: RR 4X4MM D=0.05M water/air porosity 0.6; present: sphere 6MM D=0.07M water/air porosity 0.38.

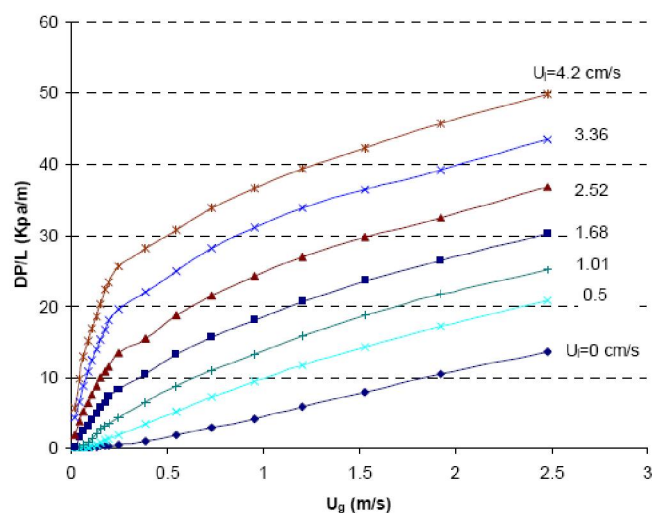


Figure 7 : Two-phase pressure gradients vs. air volumetric flux

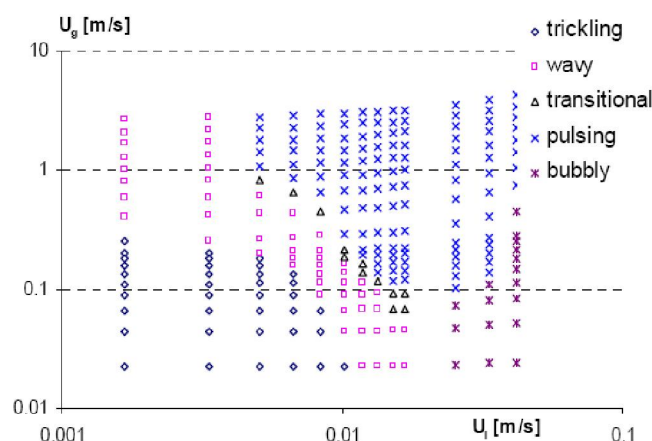


Figure 8 : Flow regime map for packed bed of diameter 0.07 and bed porosity 0.38, air-water concurrent downward flow, spherical packing of diameter 6mm

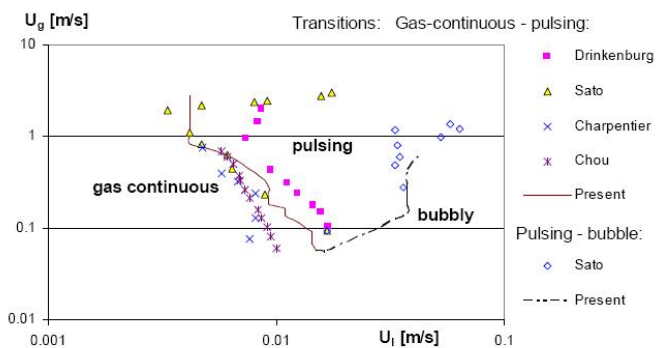


Figure 9 : Comparison of flow regime map with data of Chou (7), Drinkenburg (9), Sato (4,8) and Charpentier (22).

video. The resulting map is shown in Figure 8. Five distinct flow regimes were identified: trickling, wavy, transitional, pulsing and bubbly. The transitional flow has not often been reported in the literature. However from the high speed video images it was clear that the transition between wavy and the pulsing involves a transitional flow where occasional pulsing is observed at lower part of the test section and there is wavy flow regime throughout the test section except the lower part. In Figure 9, the current flow regime map is compared with the data of Chou (7), Drinkenburg (9), Sato (4, 8) and Charpentier (22). There is generally good agreement with flow regime observed between present work and previous research works.

CONCLUSIONS

Experiments were conducted in a trickle bed reactor for flow regime and pressure drop measurement using air water flow. In the present research, five flow regimes are observed, steady laminar trickling flow regime in which no wave or ripple can be observed directly by visual observation, wavy flow regime including ripple in part of test section, transition flow regime in which pulse happens partly and intermittently in the lower portion of the test section, pulsing flow regime and bubble flow regime. Spray flow regime was not observed in the present experiment.

ACKNOWLEDGMENT

The project was partly supported by National Research Foundation of Korea under BK 21 plus program.

Full Paper**REFERENCES**

- [1] C.N.Satterfield; *AIChE J.*, **21**, 209 (1975).
- [2] R.A.Holub, M.P.Dudukovic, P.A.Ramachandran; *AIChE J.*, **39**, 302 (1993).
- [3] V.W.Weekman Jr., E.M.John; *AIChE J.*, **10**, 951 (1964).
- [4] Y.Sato, T.Hirose; *J.Chem.Eng.Jpn.*, **6**, 147 (1973).
- [5] E.Talmor; *AIChE J.*, **23**, 868 (1977).
- [6] K.M.Ng; *AIChE J.*, **32**, 115 (1986).
- [7] T.S.Chou, F.L.Worley Jr., D.Luss; *Ind.And Eng.Chem., Proc.Design and Dev.*, **16**, 424 (1977).
- [8] Y.Sato, T.Hirose; *J.Chem.Eng.Jpn.*, **6**, 315 (1973).
- [9] A.Drinkenberg, J.R.Blok, J.Varkevisser; *Chem.Eng.Sci.*, **38**, 687 (1983).
- [10] J.C.Charpentier, M.Favier; *AIChE J.*, **21**, 1213 (1975).
- [11] V.Specchia, G.Baldi; *Chem.Eng.Sci.*, **32**, 515 (1977).
- [12] S.Fukushima, K.Kusaka; *J.Chem.Eng.Jpn.*, **11**, 241 (1978).
- [13] J.L.Turpin, R.L.Huntington; *AIChE J.*, **13**, 1196 (1967).
- [14] J.N.Al-Sheikh, D.E.Saunders, R.S.Brodkey; *Canadian J.Chem.Eng.*, **48**, 21 (1970).
- [15] A.Gianetto, G.Baldi, V.Specchia, S.Sicardi; *AIChE J.*, **24**, 1086 (1978).
- [16] O.Baker; *Oil Gas J.*, **53(12)**, 185 (1954).
- [17] S.T.Revankar, H.Holenik, D.Jo, B.Motil, *Proc.Inst.of Mech.Engineers, Part E, J.Process Mech.Eng.*, **221**, 187 (2007).
- [18] S.G.Mallat; A theory for multiresolution signal decomposition: the wavelet representation. *IEEE Trans. Pattn Anal. Mach. Intell.*, **11**, 674 (1989).
- [19] S.Ergun; *Chem.Eng.Progress*, **48(2)**, 89 (1952).
- [20] W.Hasseni, A.Laurent, N.Midou, J.C.Charpentier; *Entropie*, **23**, 127 (1987).
- [21] F.MacDonald, M.S.El-Sayed, K.Mow, F.A.L.Dullien; *Ind.And Eng.Chem.Fund.*, **18**, 199 (1979).
- [22] J.C.Charpentier; *Chem.Eng.J.*, **11(3)**, 161 (1976).